

A discrete time-dependent method for metastable atoms in intense fields

Liang-You Peng^{*,†}, J F McCann[†], Daniel Dundas[†], K T Taylor[†] and I D Williams[†]

^{*}International Research Centre for Experimental Physics,

[†]School of Mathematics and Physics,

Queen's University Belfast,

Belfast BT7 1NN, Northern Ireland, UK.

The full-dimensional time-dependent Schrödinger equation for the electronic dynamics of single-electron systems in intense external fields is solved directly using a discrete method. Our approach combines the finite-difference and Lagrange mesh methods. The method is applied to calculate the quasienergies and ionization probabilities of atomic and molecular systems in intense static and dynamic electric fields. The gauge invariance and accuracy of the method is established. Applications to multiphoton ionization of positronium and hydrogen atoms and molecules are presented. At very high intensity above saturation threshold, we extend the method using a scaling technique to estimate the quasienergies of metastable states of the hydrogen molecular ion. The results are in good agreement with recent experiments.

I. INTRODUCTION

Matter exposed to intense laser fields has attracted extensive research in the past two decades. Due to the competition between external forces induced by the laser field and Coulomb interactions, which bind the system together, the nature of the metastable states that arise is strongly controlled by the nature of the external field and is not simply a feature of the atomic or molecular system. In such circumstances the internal and external fields are on an equal footing and not separable.

The study of these effects in few-electron atoms have become accessible recently both experimentally and theoretically because of advances in experimental techniques and the availability of supercomputers. Compared with atoms, molecules in intense laser fields are much more complicated not only because of the multi-center nature of the problem but also due to the additional vibrational and rotational degrees of freedom associated with the nuclei [1, 2]. In polyatomic systems, the energy transfer to collective motion leads to extremely high-energy secondary photons, ions and electrons [3, 4].

Standard perturbation theory is no longer applicable when the forces induced by the applied laser field are comparable to the binding forces of the system. If the external field is periodic then the system is metastable and has a well-defined quasienergy spectrum. Suppose the unperturbed ground-state has a real energy E_i , then the effect of the external field is to produce an energy shift Δ and decay width rate Γ/\hbar , so that the quasienergy has the usual form $E = E_i + \Delta - i\Gamma/2$. This describes a steady-state decay and can be treated very effectively with time-independent methods such as the Floquet method. However, at the very highest intensities the transient aperiodic effects of short duration pulses of dynamic fields mean that the shift and rate are poorly defined. Under these conditions a time-dependent approach is essential. In this paper we describe such an approach applied to the regimes where the quasienergy is well-defined and to time-dependent problems where this is not the case. We find the method works efficiently and accurately for both cases, and thus is well-suited to the study of metastable states under all conditions.

Recent advances in experimental technology in the utilisation of high intensity lasers have led to the creation and study of short-lived atomic and molecular states. In this paper we apply the method to problems of this type, though the method is of more general applicability. With very short pulses, not only the laser envelope but even the phase of the field can be important [5]. Therefore, one has to directly integrate the full-dimensional Schrödinger equation in order to describe accurately the underlying physical mechanisms [6, 7, 8] and obtain data relevant to experiments.

Although one-dimensional models have been routinely used in describing atoms and molecules in strong laser fields [9], *ab initio* full-dimensional quantum-mechanical calculations are very important for exactly calculable few-electron systems. As discussed in [9], the numerical results for excitation, dissociation and ionization in simplified models are strongly sensitive to the parameters chosen. Full-dimensionality calculations without approximation are really necessary to establish accurate data as benchmarks to assess the quality or regime of applicability of other calculations and to produce results which are comparable with experimental observations.

We have recently developed a very accurate and efficient numerical method to study metastable states in high intensity fields. This was applied to the fragmentation of the hydrogen molecular ion in an intense laser field beyond the Born-Oppenheimer approximation [8, 10, 11]. In this paper, we make a detailed investigation of this method applied to metastable atomic and molecular systems. We discuss the variational characteristics of this method and confirm its accuracy, convergence and gauge invariance. Results are compared to other theoretical estimates of the metastable states, and we compare with experimental results for the ionization of the hydrogen molecular ion at high intensities.

II. DISCRETE TIME-DEPENDENT SCHRÖDINGER EQUATION

Our goal is the direct solution of the time-dependent Schrödinger equation of an arbitrary one-electron systems in

strong external electric fields

$$H_e \Psi_e(\mathbf{r}, t) = i\hbar \frac{\partial}{\partial t} \Psi_e(\mathbf{r}, t), \quad (1)$$

where

$$H_e \equiv \frac{1}{2m_e} (\mathbf{p} + e\mathbf{A}(\mathbf{r}, t))^2 + V(\mathbf{r}, t), \quad (2)$$

and $\mathbf{A}(\mathbf{r}, t)$ is the (external) vector potential; $V(\mathbf{r}, t)$ is the (internal) scalar potential. An example of such a problem is a one-electron molecular system in an intense laser field; the internal field arising from the positively-charged nuclei. In order to simplify the model and to understand the electronic dynamics in isolation, we consider the hydrogen molecular ion with the nuclei fixed in space. The nuclei, labelled 1 and 2, are a fixed distance R apart, and have charges Z_1 and Z_2 . The origin of the coordinate \mathbf{r} is located at the internuclear midpoint, with the electronic Hamiltonian takes the form

$$H_e \equiv \frac{1}{2m_e} (\mathbf{p} + e\mathbf{A}(\mathbf{r}, t))^2 + \frac{e^2}{4\pi\epsilon_0} \left(-\frac{Z_1}{r_1} - \frac{Z_2}{r_2} + \frac{Z_1 Z_2}{R} \right), \quad (3)$$

with $r_1 = |\mathbf{r} + \frac{1}{2}\mathbf{R}|$ and $r_2 = |\mathbf{r} - \frac{1}{2}\mathbf{R}|$, and \mathbf{A} the vector potential. We include the constant internuclear potential for reasons of convention. Removing the quadratic term $(e^2/2m_e)\mathbf{A}^2$ by gauge transformation, and making the dipole approximation, the Hamiltonian in the Coulomb gauge can be written as

$$H_e^{(V)} \equiv \frac{1}{2m_e} \mathbf{p}^2 + \frac{e}{m_e} \mathbf{A}(t) \cdot \mathbf{p} + \frac{e^2}{4\pi\epsilon_0} \left(-\frac{Z_1}{r_1} - \frac{Z_2}{r_2} + \frac{Z_1 Z_2}{R} \right), \quad (4)$$

while in the length gauge: $\mathbf{E}(t) = -\partial\mathbf{A}/\partial t$

$$H_e^{(L)} \equiv \frac{1}{2m_e} \mathbf{p}^2 + e\mathbf{r} \cdot \mathbf{E}(t) + \frac{e^2}{4\pi\epsilon_0} \left(-\frac{Z_1}{r_1} - \frac{Z_2}{r_2} + \frac{Z_1 Z_2}{R} \right). \quad (5)$$

Monochromatic light with linear polarization parallel to the internuclear axis implies a cylindrical symmetry about this axis. Associated with this symmetry is a good quantum number, Λ , proportional to the projection of angular momentum along the axis. Thus the electron position can be completely described by the radial, ρ , and axial, z , coordinates with respect to an origin taken at the midpoint between the nuclei. The time-dependent Schrödinger equation reduces to a 2+1 dimensional partial differential equation. Hence in atomic units

$$H_e^{(L)}(R; \rho, z; t) = -\frac{1}{2} \left(\frac{\partial^2}{\partial z^2} + \frac{\partial^2}{\partial \rho^2} + \frac{1}{\rho} \frac{\partial}{\partial \rho} \right) + V_m(R, \rho, z) + V_{\text{ml}}^{(L)}(z, t), \quad (6)$$

where the electronic potential energy is the non-separable singular function

$$V_m(R, \rho, z) = -\frac{Z_1}{\sqrt{\rho^2 + (z + \frac{1}{2}R)^2}} - \frac{Z_2}{\sqrt{\rho^2 + (z - \frac{1}{2}R)^2}} + \frac{\Lambda^2}{2\rho^2} + \frac{Z_1 Z_2}{R}, \quad (7)$$

and the molecule-laser interaction term is

$$V_{\text{ml}}^{(L)}(z, t) = zE(t). \quad (8)$$

Consider a short optical pulse that is approximately monochromatic, within the bandwidth limit, with a well-defined peak intensity. This can be simulated by choosing an electric field of the following form

$$E(t) = E_0 f(t) \cos \omega_L t, \quad (9)$$

where the pulse envelope, $f(t)$, is given by

$$f(t) = \begin{cases} \frac{1}{2} \left[1 - \cos \left(\frac{\pi t}{\tau_1} \right) \right] & 0 \leq t \leq \tau_1 \\ 1 & \tau_1 \leq t \leq \tau_1 + \tau_2 \\ \frac{1}{2} \left[1 - \cos \left(\frac{\pi(t - \tau_2 - 2\tau_1)}{\tau_1} \right) \right] & \tau_1 + \tau_2 \leq t \leq \tau_2 + 2\tau_1 \\ 0 & t < 0, t > \tau_2 + 2\tau_1 \end{cases} \quad (10)$$

and in which E_0 is the peak electric field, the pulse ramp time is τ_1 and the pulse duration τ_2 , with associated bandwidth $\Delta\omega = 1/\tau_2$. Since the peak field, E_0 , is related to the cycle-average intensity, $\langle I \rangle$, by the relation $\langle I \rangle = \frac{1}{2} c \epsilon_0 E_0^2$ then the conversion formula is $E_0 \approx 5.338 \times 10^{-9} \sqrt{\langle I \rangle}$ if the intensity $\langle I \rangle$ is in W cm^{-2} , and the field strength in atomic units. The corresponding ponderomotive energy is $U_P = E_0^2 / (4\omega_L^2)$. Consider the molecule initially in the ground state $X^2\Sigma_g^+$. It is convenient to change the dependent variable to remove the first-derivative in ρ as follows

$$\phi(\rho, z, t) = (2\pi\rho)^{1/2} \psi(\rho, z, t), \quad (11)$$

so that the time-dependent equation is

$$i \frac{\partial}{\partial t} \phi(\rho, z, t) = [T_z + T_\rho + V_m(\rho, z, R) + V_{\text{ml}}^{(L)}(z, t)] \phi(\rho, z, t), \quad (12)$$

where

$$T_\rho \equiv -\frac{1}{2} \left(\frac{\partial^2}{\partial \rho^2} + \frac{1}{4\rho^2} \right), \quad T_z \equiv -\frac{1}{2} \left(\frac{\partial^2}{\partial z^2} \right), \quad (13)$$

with the normalization convention

$$\int_0^\infty d\rho \int_{-\infty}^{+\infty} dz |\phi(\rho, z, 0)|^2 = 1. \quad (14)$$

This 2+1 dimensional equation, given in Eq. (12), can be discretized on an $N_\rho \times N_z \times N_t$ space-time grid. We label the N_ρ radial nodes by, $\{\rho_1, \rho_2, \dots, \rho_i, \dots, \rho_{N_\rho}\}$, while the N_z axial grid points are denoted by, $\{z_1, z_2, \dots, z_j, \dots, z_{N_z}\}$. The evolution progresses through the sequence of times $\{t_1, t_2, \dots, t_k, \dots, t_{N_t}\}$. Thus the wavefunction can be written as the array $\phi(\rho, z, t) \rightarrow \phi(\rho_j, z_i, t_k) \equiv \phi_{ijk}$. The method of discretization of the Hamiltonian divides the axial and radial coordinates into subspaces. Two distinct but complementary grid methods are used for the subspaces. The radial subspace is discretized over a semi-infinite range using a small number N_ρ of unevenly spaced points that are the nodes of global interpolating functions that enter the Lagrange mesh technique. This leads to a small dense matrix for the Hamiltonian in the ρ -subspace. On the other hand the axial coordinate subspace is represented by a large number of equally-spaced points that are the mesh points of a finite-difference scheme. The associated subspace Hamiltonian matrix is large but sparse. Our approach is tailored to the requirements of accuracy and computational efficiency.

A. Discretization of the Hamiltonian in the radial subspace

For wavefunction character in the ρ -coordinate we have found that a Lagrange mesh [8, 12] can provide a more efficient discretization scheme compared with that provided by finite-difference formulae. This type of grid can be chosen to accommodate short-range singularities or long-range behaviour, and can be scaled in length or number of grid points to improve accuracy with a modest number of points. We rescale the radial variable as follows, $\rho = hx$ where h is some arbitrary scaling factor, and $0 \leq x < +\infty$. Then consider the set of functions

$$\varphi_n(x) = \left(\frac{n!}{\Gamma(\alpha + n + 1)} \right)^{1/2} x^{\alpha/2} e^{-x/2} L_n^{(\alpha)}(x), \quad (15)$$

where $L_n^{(\alpha)}(x)$ are the generalized Laguerre polynomials

$$L_n^{(\alpha)}(x) \equiv \frac{1}{n!} e^x x^{-\alpha} \frac{d^n}{dx^n} (e^{-x} x^{\alpha+n}). \quad (16)$$

These functions form an orthonormal set on the domain $0 \leq x < \infty$

$$\int_0^\infty \varphi_m(x) \varphi_n(x) dx = \delta_{mn}. \quad (17)$$

Then, for any given value of α , one can construct an N_ρ -point grid based upon Gauss quadrature rules. Choosing the grid points $(x_1, x_2, \dots, x_{N_\rho})$ as the N_ρ solutions of $L_{N_\rho}^{(\alpha)}(x) = 0$, the quadrature weights corresponding to these pivots are given by the Christoffel numbers λ_i , where

$$\lambda_i^{-1} = x_i \varphi'_{N_\rho}(x_i)^2. \quad (18)$$

One can define the set of differentiable functions

$$f_i(x) = \lambda_i^{-1/2} \left(\frac{1}{\varphi'_{N_\rho}(x_i)} \right) \frac{\varphi_{N_\rho}(x)}{x - x_i}, \quad (19)$$

where these mesh functions have properties both of Lagrange interpolation functions and exact discrete orthogonality, that can be summarised as follows

$$\lambda_i^{1/2} f_i(x_j) = \delta_{ij}, \quad (20)$$

$$\sum_{k=1}^{N_\rho} \lambda_i f_i(x_k) f_j(x_k) = \delta_{ij}. \quad (21)$$

The matrix element of an operator or function $Q(x, \frac{\partial}{\partial x})$, in this basis is given by

$$\int_0^\infty f_i^*(x) Q(x, \frac{\partial}{\partial x}) f_j(x) dx = \lambda_i^{-1/2} \left[Q(x, \frac{\partial}{\partial x}) f_j(x) \right]_{x_i} + \varepsilon \quad (22)$$

where the error, ε , in the Gaussian quadrature depends on N_ρ , α and the form of Q . Expanding the wave function in this basis

$$\phi(\rho, z, t) = \sum_{i=1}^{N_\rho} (\lambda_i)^{1/2} \phi(hx_i, z, t) f_i(x), \quad (23)$$

In the radial subspace the kinetic energy is represented by the dense matrix [12]

$$(T_\rho)_{il} = \begin{cases} \frac{1}{2h^2} \left(\frac{(\alpha+1)^2}{4x_i^2} + S_{ii} \right), & i = l \\ \frac{(-1)^{i-l}}{2h^2} \left[\frac{1}{2} \frac{\alpha+1}{\sqrt{x_i x_l}} \left(\frac{1}{x_i} + \frac{1}{x_l} \right) + S_{il} \right], & i \neq l \end{cases} \quad (24)$$

with

$$S_{il} = (x_i x_l)^{1/2} \sum_{k \neq i, l} x_k^{-1} (x_k - x_i)^{-1} (x_k - x_l)^{-1}. \quad (25)$$

Then the Hamiltonian in the radial subspace has the form

$$(H_z)_{il} \equiv \delta_{il} (T_z) + (T_\rho)_{il} + \delta_{il} V_m(\rho_i, z, R) + \delta_{il} V_{ml}(z, t). \quad (26)$$

The last grid point, the largest root of $L_{N_\rho}^{(\alpha)}(\rho/h) = 0$, defines ρ_{\max} , the radius of the cylindrical box.

B. Discretization of the Hamiltonian in the axial subspace

The axial coordinate grid is chosen to be a set of N_z equally spaced points which cover the range $-z_{\max} \leq z \leq z_{\max}$ with a separation $\Delta z = 2z_{\max}/(N_z - 1)$, so that $z_j = -z_{\max} + (j - 1)\Delta z$. We choose the method of finite differences to treat this coordinate in order to make effective use of parallel processing and for appropriate treatment of wavefunction dependence on z [13]. The sparsity of the matrix and confinement of communication to that between nearest neighbours is ideal for efficient calculation. For example, the

kinetic energy can be evaluated by the five-point finite central difference formula

$$(T_z)_{jm} = \frac{1}{24(\Delta z)^2} (\delta_{j+2,m} - 16\delta_{j+1,m} + 30\delta_{jm} - 16\delta_{j-1,m} + \delta_{j-2,m}), \quad (27)$$

with error proportional to $(\Delta z)^4$ and resulting in a sparse (pentadiagonal) matrix. The momentum operator arises in the velocity gauge perturbation and is given by

$$\left[V_{\text{ml}}^{(V)} \right]_{jm} = \frac{-iA(\rho_i, t)}{12(\Delta z)} (-\delta_{j+2,m} + 8\delta_{j+1,m} - 8\delta_{j-1,m} + \delta_{j-2,m}), \quad (28)$$

with error proportional to $(\Delta z)^5$.

Therefore the augmented $(N_\rho \times N_z) \times (N_\rho \times N_z)$ Hamiltonian matrix takes the form

$$\begin{aligned} \left[H_e^{(L)}(t) \right]_{il,jm} &\equiv \delta_{il} (T_z)_{jm} + (T_\rho)_{il} \delta_{jm} \\ &+ \delta_{il} \delta_{jm} V_m(\rho_i, z_j, R) \\ &+ \delta_{il} \delta_{jm} V_{\text{ml}}^{(L)}(z_j, t), \end{aligned} \quad (29)$$

in the length gauge and

$$\begin{aligned} \left[H_e^{(V)}(t) \right]_{il,jm} &\equiv \delta_{il} (T_z)_{jm} + (T_\rho)_{il} \delta_{jm} \\ &+ \delta_{il} \delta_{jm} V_m(\rho_i, z_j, R) \\ &+ \delta_{il} \left[V_{\text{ml}}^{(V)}(z_j, t) \right]_{jm}, \end{aligned} \quad (30)$$

in the velocity gauge.

C. Discretization and propagation in time

The wavefunction is discretized on a grid so that it makes up a vector of $N_\rho \times N_z$ components. At time t_k the (i, j) th element of the vector \mathbf{v}_k can be defined as

$$(\mathbf{v}_k)_{i,j} = \phi(hx_i, z_j, t_k), \quad (31)$$

while the (il, jm) th element of the matrix \mathbf{H}_k is defined

$$(\mathbf{H}_k)_{il,jm} = [H(t_k)]_{il,jm}, \quad (32)$$

so that the time evolution is described by the equation

$$\mathbf{H}(t)\mathbf{v}(t) = i\dot{\mathbf{v}}(t). \quad (33)$$

Suppose that time is divided so that $t_{k+1} \equiv t_k + \Delta t$ then the solution can be propagated using the unitary evolution matrix

$$\mathbf{v}_{k+1} \equiv \mathbf{U}(t_k + \Delta t, t_k)\mathbf{v}_k \approx \exp(-i\mathbf{H}_k \Delta t)\mathbf{v}_k. \quad (34)$$

Evaluation of this exponential is carried out using a Krylov subspace decomposition [7, 8]. Using the Arnoldi algorithm [14] we construct an orthonormal set of vectors, $[\mathbf{q}_0, \mathbf{q}_1, \mathbf{q}_2, \dots, \mathbf{q}_{n_a}]$, which span the Krylov subspace

$$K_{n_a}(\mathbf{H}_k, \mathbf{v}_k) \equiv \text{span} \{ \mathbf{v}_k, \mathbf{H}_k \mathbf{v}_k, \mathbf{H}_k^2 \mathbf{v}_k, \dots, \mathbf{H}_k^{n_a} \mathbf{v}_k \}. \quad (35)$$

The orthonormal set is formed using Gram-Schmidt orthogonalization. Letting \mathbf{h}_k denote the $(n_a + 1) \times (n_a + 1)$ upper-Hessenberg matrix formed by the coefficients $(\mathbf{h}_k)_{ij}$ we obtain the matrix equation

$$\mathbf{h}_k = \mathbf{Q}_k^\dagger \mathbf{H}_k \mathbf{Q}_k, \quad (36)$$

where \mathbf{Q}_k is a matrix formed from the n_a column vectors $[\mathbf{q}_0, \mathbf{q}_1, \mathbf{q}_2, \dots, \mathbf{q}_{n_a}]$ and so \mathbf{h}_k is the Krylov subspace Hamiltonian which is calculated simultaneously with \mathbf{Q}_k . $\tilde{\mathbf{H}}_k = \mathbf{Q}_k^\dagger \mathbf{H}_k \mathbf{Q}_k$ can be used as a replacement to \mathbf{H}_k in a wide variety of applications. In particular the time-evolution operator can be written as

$$\tilde{\mathbf{U}}(t_k + \Delta t, t_k) = e^{-i\tilde{\mathbf{H}}_k \Delta t} = \mathbf{Q}_k e^{-i\mathbf{h}_k \Delta t} \mathbf{Q}_k^\dagger. \quad (37)$$

Now \mathbf{h}_k is typically a tridiagonal matrix and so $e^{-i\mathbf{h}_k \Delta t}$ can be computed inexpensively. Thus $\tilde{\mathbf{U}}(t_k + \Delta t, t_k)$ is in effect a unitary propagator correct to order $(\Delta t)^{n_a}$.

III. ACCURACY OF THE DISCRETE SOLUTIONS

The results we obtain from this method depend on several parameters, namely N_ρ , h_ρ , Δz , z_{max} , n_a , Δt , and the choice of gauge used to describe the laser-molecule interaction term. In this section we detail the choices for these parameters required to obtain accurate and fully converged solutions.

A. Spatial grid parameters

In an intense field problem, the dynamics of the system can be very sensitive to the initial state. Therefore, the accuracy of the ground state wavefunction and its corresponding energy play a crucial role. Several important grid parameters are open to choice, and to determine these we proceed as follows. We first choose the values of Δz and N_ρ , then apply a variational method by adjusting the value of $0 \leq h_\rho \leq 2$ until we get an accurate ground-state energy. Importantly, once this procedure is completed for a specific internuclear distance R , the same scaling factor works well for all R . In this hybrid finite-difference/discrete-variable method we noted that there is a delicate relation among the values of Δz , N_ρ and h_ρ . For a fixed N_ρ value, if we double the value Δz , we have to roughly double the value of h_ρ in order to maintain accurate energies. Since the kinetic energy terms are homogeneous in these coordinates this maintains the balance between these terms. In the following calculations, we take the range of the z coordinate as $[-z_{\text{max}}, z_{\text{max}}]$, where $z_{\text{max}} = 300.9$ a.u. and $\Delta z = 0.1$ a.u. (6019 points in all). The z -subspace is shared across the processor array, in our case we used 13 processors for this task. The ρ -subspace is spanned fully on each processor and we take $N_\rho = 30$ with $h_\rho = 0.5185$ corresponding to the limit $\rho_{\text{max}} \sim 55$ a.u.

To obtain the ground state eigenvectors it is convenient and efficient to use an iterative Lanczos method [8]. In Table I, we list our ground state energies for $\Lambda = 0$ and $\Lambda = 1$ at different

TABLE I: Calculated energies for the lowest states of gerade symmetry with $\Lambda = 0$ and $\Lambda = 1$ for different R , compared with the exact values from Sharp's tabulation [15]. Values of R and energy are in atomic units.

R	$\Lambda = 0$ state		$\Lambda = 1$ state	
	Exact	Present	Exact	Present
1.0	-0.451785	-0.451783	0.525893	0.525872
2.0	-0.602635	-0.602636	0.071229	0.071216
4.0	-0.546085	-0.546088	-0.100825	-0.100830
6.0	-0.511968	-0.511972	-0.130325	-0.130327
8.0	-0.502570	-0.502574	-0.134511	-0.134512
10.0	-0.500580	-0.500582	-0.132716	-0.132716
12.0	-0.500167	-0.500172	-0.129950	-0.129948
16.0	-0.500035	-0.500040	-0.126253	-0.126243
20.0	-0.500015	-0.500018	-0.125084	-0.125072

internuclear distances and compare them with the exact values from Sharp's tabulation. Here, we have taken $\Delta z = 0.1$ a.u. and $N_\rho = 30$ in both calculation. However, the scaling parameter h_ρ has been adjusted to 0.5185 for $\Lambda = 0$ and 0.146 for $\Lambda = 1$, these values are used for all R in the table. The results are in excellent agreement compared with the exact results.

The excited state spectrum supported by the grid can be found using the spectrum of the autocorrelation function [8]

$$C(t) = \int d^3\mathbf{r} \phi^*(\mathbf{r}, t) \phi(\mathbf{r}, 0), \quad (38)$$

where $\phi(\mathbf{r}, 0)$ is an arbitrary trial function, and $\phi(\mathbf{r}, t)$ is the function evolved in the field-free Hamiltonian $\phi(\mathbf{r}, t) = \exp(-iH_0t/\hbar)\phi(\mathbf{r}, 0)$. The natural frequencies (eigenenergies) appear as peaks in the spectral density

$$P(\omega, T) = \left| \int_0^T C(t) e^{i\omega t} dt \right|^2. \quad (39)$$

The resolution improves with longer times, T . The trial function can be chosen to find the states of given symmetry. We have compared the energies of the electronic states at an equilibrium separation $R = 2.0$ a.u. with the exact results given by Sharp [15]; this comparison was previously performed by Dundas [8]. Our current results are more accurate and better resolved than those given in [8]. This has been achieved using a finer axial grid $\Delta z = 0.1$ a.u. as compared with $\Delta z = 0.2$ a.u. [8], but also by adjustment of the scaling factor h_ρ . By trial and error, we determined that $h_\rho \approx 0.5185$ gave the best estimates over the full spectrum. The scaling factor can be considered a variational parameter [12]. This is a useful and reliable method to determine the optimal grid parameters for subsequent dynamic calculations.

At the very least, the dimensions of the cylindrical box, height $2z_{\max}$ radius ρ_{\max} , must be chosen to encompass the tightly-bound states of the system. However, the evolution through highly-excited diffuse states and low-energy continuum states is crucial to the ionization mechanism at low frequencies. The rescattering mechanism, by which slow photoelectrons are driven back to the core region by the laser field,

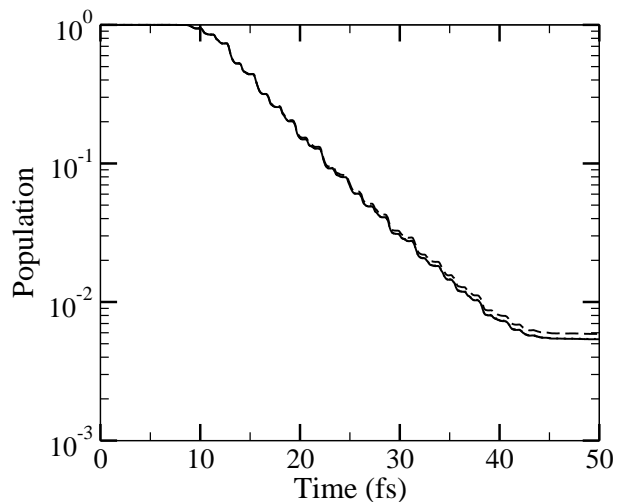


FIG. 1: Population loss for different time steps Δt . The characteristics of the laser pulse are, $\lambda = 800$ nm, $I = 3.2 \times 10^{14}$ W cm^{-2} , with $\tau_1 = 5$ cycles (13.4fs) and $\tau_2 = 10$ cycles (26.7 fs) and the bond length is $R = 5$ a.u. The curves correspond to: — $\Delta t = 0.02$; $\dots\dots$ $\Delta t = 0.04$; - - - $\Delta t = 0.06$ in atomic units.

means that the box size should be large enough to allow the continuum states to evolve unfettered. For example, the free-electron classical amplitude of displacement and momentum are proportional to E_0/ω_L^2 and E_0/ω_L , respectively and so box dimensions of several hundred atomic units may be required.

The boundary between bound and free electrons was established in two ways. We have defined an inner region which satisfies either

$$\sqrt{\rho^2 + (z - R/2)^2} \leq r_{\text{inner}}, \quad (40)$$

or

$$\sqrt{\rho^2 + (z + R/2)^2} \leq r_{\text{inner}}, \quad (41)$$

where R is the internuclear separation distance and r_{inner} is taken to be 20 a.u. We also define an outer box population to be the total population within the entire grid.

In order to prevent reflection of ionizing wavefunction from the edges of the grid wavefunction splitting which acts in the same manner as an absorbing potential is applied in both the z and ρ directions [8].

B. Time propagation parameters

A 12-th order Arnoldi propagator ($n_a = 12$) was used in these calculations. A test of the method for numerical stability with respect to the time step, Δt using this choice of propagator order, n_a , in conjunction with the spatial grid parameters outlined above is given in figure 1. The logarithmic scale accentuates the differences in the residual population at the end of the pulse. In this case we note the very good convergence of the method. Results are presented for the following case:

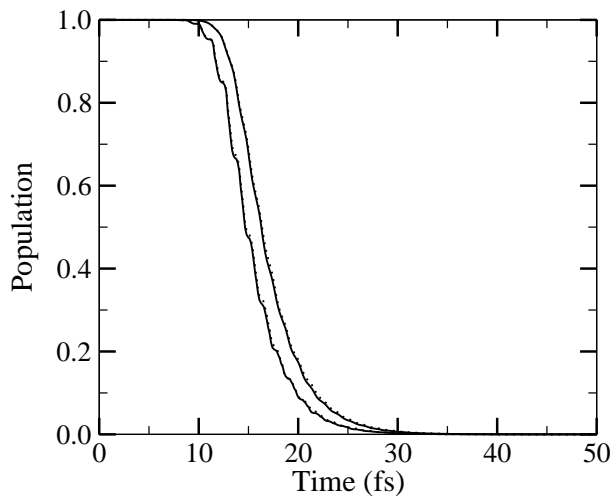


FIG. 2: Electron population within the inner and outer boxes for length (full lines) and velocity (dotted lines) gauges. The two curves to the left correspond to the inner box, those to right, to the outer box. The bond length is $R = 6$ a.u., and the laser pulse parameters are $\lambda = 800$ nm and $I = 3.2 \times 10^{14}$ W cm $^{-2}$ with $\tau_1 = 5$ cycles (13.4fs) and $\tau_2 = 10$ cycles (26.7fs).

$\lambda = 800$ nm and $I = 3.2 \times 10^{14}$ W cm $^{-2}$, and with $\tau_1 = 5$ cycles (13.4 fs) and $\tau_2 = 10$ cycles (26.7fs) with $R = 5$ a.u. On this figure we note that only the largest time step $\Delta t = 0.06$ a.u. produces a small but discernible deviations in the results. We find that $\Delta t = 0.05$ a.u. is sufficient for convergence in most cases, however the range $\Delta t = 0.01 - 0.03$ a.u. provides more reliable and accurate results.

C. Gauge invariance

In Fig. 2, we show the populations within the inner and outer boxes in both length gauge and velocity gauge. The bond length is $R = 6$ a.u., and the laser pulse parameters are $\lambda = 800$ nm and $I = 3.2 \times 10^{14}$ W cm $^{-2}$ with $\tau_1 = 5$ cycles and $\tau_2 = 10$ cycles. Excellent agreement between both gauges is observed. This agreement also extends to longer wavelengths and longer bond lengths.

IV. RESULTS

A. Static field ionization rates

The static field ionization rates of the hydrogen atom and molecular ions are known to a high degree of accuracy using time-independent methods and provide an important test of our method. In our time-dependent approach the field is switched on over a time $\tau_1 = 2$ fs, with the static field maintained at a constant value F for $\tau_2 = 6$ fs. The rise in the field should be slow enough to ensure an adiabatic transition for the field-free ground state to the metastable state. In table II, we compare our results for the atom field ionization rates with the

TABLE II: Static-field ionization rates Γ for the hydrogen atom. Comparison between time-independent (Floquet) calculations [17] and time-dependent methods (this work). The electric field strength F is given in atomic units. The ionization rates are quoted in the format $a(n) \equiv a \times 10^n$ fs $^{-1}$.

F (a.u.)	0.1	0.08	0.06	0.05338	0.04
Floquet	0.601(0)	0.188(0)	0.213(-1)	0.664(-2)	0.162(-3)
Present	0.600(0)	0.188(0)	0.213(-1)	0.664(-2)	0.163(-3)

highly accurate time-independent results [16, 17]. Very good agreement is obtained in all cases.

The same method can be applied to the molecular ion. However in this case the comparison is not so straightforward. Plummer and McCann [16] noted that at large bond lengths the nearly degenerate pair of $\Sigma_{g,u}$ field-free states are strongly split by the external field. The correlated eigenstates are a pair of localised atomic resonances with large differences in their energies and their widths γ_1, γ_2 . If we apply a static field over a time $\tau_1 = 5$ fs, relatively short in comparison to that characterising the gerade-ungerade splitting, that is the hopping time for the electron between the centers, then the electron divides equally between the atom sites, creating an equal mixture of the resonance states rather than an adiabatic transfer to one or other state. Since $\gamma_1 \gg \gamma_2$ this would imply that half of the population is trapped. Consider the duration of the static field T_s such that $\gamma_1 \ll T_s^{-1}$, then the population decay in the time-dependent model is given by $\Gamma = -dP/dt \approx \frac{1}{2}\gamma_1$, where γ_1 is the width of the short-lived state. If this were the case, then at longer times $T_s \gg \gamma_1^{-1}$ but $T_s \ll \gamma_2^{-1}$ the population should reach a limit of 0.5. Figure 3 shows the population as a function of time with $\tau_1 = 5$ fs and $\tau_2 = 390$ fs for $F = 0.04$ and $R = 11$. The population decays gradually to a limiting value of 0.5 as predicted. However when the data is

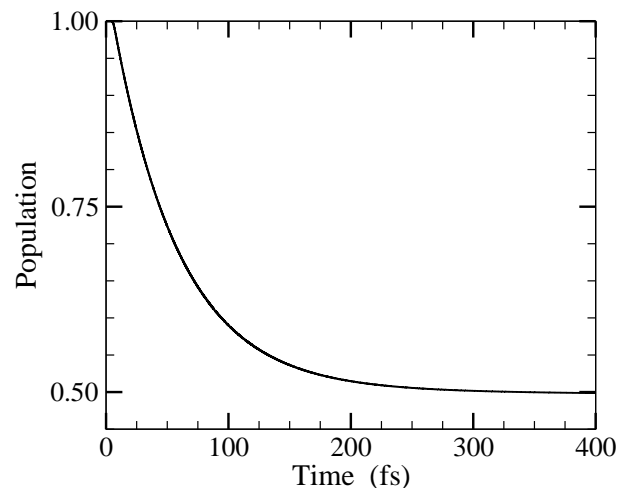


FIG. 3: Electron bound-state population as a function of time for the H_2^+ ion. Static electric field strength $F = 0.04$ a.u., internuclear distance $R = 11$ a.u.. At longer times (> 200 fs) the decay is inhibited by a trapped state created during the rise of the electric field over a time $\tau_1 = 5$ fs.

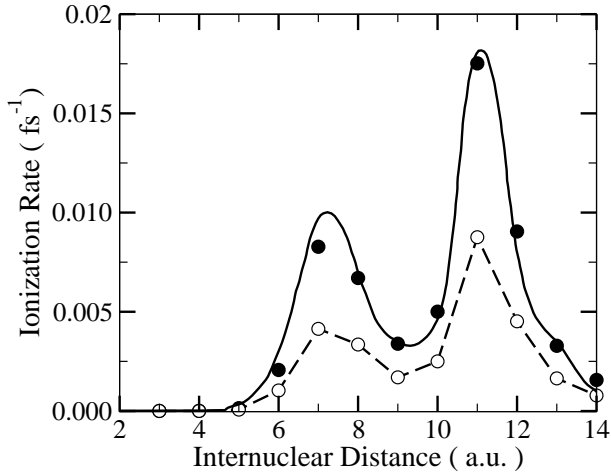


FIG. 4: Ionization rate Γ of H_2^+ as a function of internuclear distance R in a static electric field $F = 0.04$ a.u. The results show that for the large bond lengths, the electron splits evenly into a long-lived trapped state (g) and a short-lived resonance (u): —, Floquet calculation [16] for the u state; ●, present calculation $\times 2$; ○, present calculation.

plotted on a logarithmic scale we notice that the decay process is not purely exponential. At the beginning, between 8 fs and 13 fs, we estimate the ionization rate to be $8.75 \times 10^{-3} \text{ fs}^{-1}$ and near the end $3.91 \times 10^{-5} \text{ fs}^{-1}$ between 390 fs and 395 fs. The ionization rate calculated by the Floquet method is $1.76 \times 10^{-2} \text{ fs}^{-1}$ for the u -state and $2.57 \times 10^{-5} \text{ fs}^{-1}$ for the g -state [16]. The factor of 2 difference is consistent with the wavefunction splitting and population trapping. Further evidence is provided in figure 4, with ionization rates as a function of R , compared with those results obtained by Plummer and McCann [16] for the rate γ_1 . At larger R values the splitting is almost exactly one half in agreement with the adiabatic trapping model. However, at smaller values of R we note that the degeneracy of the molecular states is removed and the ionization drops rapidly as the electron is able to move adiabatically into the trapped state.

B. Energy shift of metastable states

The method can be applied to calculate the real part of the quasienergy, that is the Stark shift of the levels. In this case, we calculate the autocorrelation function $C(t)$ for a trial function evolving with the external field on. We first calculate the shifts for the hydrogen atom and compare with other well-established results. In table III, results are compared with those obtained by the complex-coordinate approach [18] for a static field DC Stark effect. Very good agreement is achieved. The resolution in the time-dependent method is limited by the bandwidth theorem: $\Delta\omega \approx 1/T_p$, where T_p is the duration of the pulse. The calculation of the AC Stark shift is done in the same way. We compare with the Floquet method applied to the hydrogen atom [18] for the angular frequency

TABLE III: Stark shifts Δ for the hydrogen atom ground state. The electric field amplitude F_0 and laser angular frequencies are given in atomic units. $\omega_L = 0$ corresponds to the static field.

F_0	0.10	0.0354
ω_L	0	0.375
Present results	-0.02746	-0.0117
Floquet method [18]	-0.02742	-0.0119

$\omega_L = 0.375$. This is exactly resonant with the $2p_z$ state and thus, for moderate or low intensities, the AC Stark shift is to a good approximation half the Rabi frequency for the transition, that is

$$\Delta \approx -\frac{1}{2}F_0 \int d^3\mathbf{r} \phi_{1s}(\mathbf{r}) z \phi_{2p_z}(\mathbf{r}) \quad (42)$$

where ϕ_{1s} and ϕ_{2p_z} are the $1s$ and $2p_z$ wavefunctions respectively for the hydrogen atom, F_0 is the maximum of the electric field strength. For $F_0 = 0.0354$ a.u. then $\Delta \approx -0.0132$ a.u. A more precise estimate using our code is -0.0117 a.u., which is in good agreement with the result of Maquet *et al* [18] $\Delta = -0.0119$ (see table III). Consider now the quasienergies of the molecular ions. In figure 5 the spectral density for $R = 2$ a.u. is given for the laser parameters $\lambda = 800$ nm, $I = 5 \times 10^{14} \text{ W cm}^{-2}$. In this case, the periodicity of the Floquet spectrum is clearly visible: $E_i + \Delta \pm n\omega_L$. The periodicity is extended and the peaks become sharper as the duration of the pulse increases. However, the resolution is limited by broadening due to the ionization process. The gap between any two neighbouring peaks is exactly one photon energy, i.e., 0.057 a.u. for the present case. From the data we estimate the Stark shift for the ground state is $\Delta_g = -0.018$ a.u. and for the first excited state $\Delta_u = -0.0075$ a.u. The quasienergy spectrum

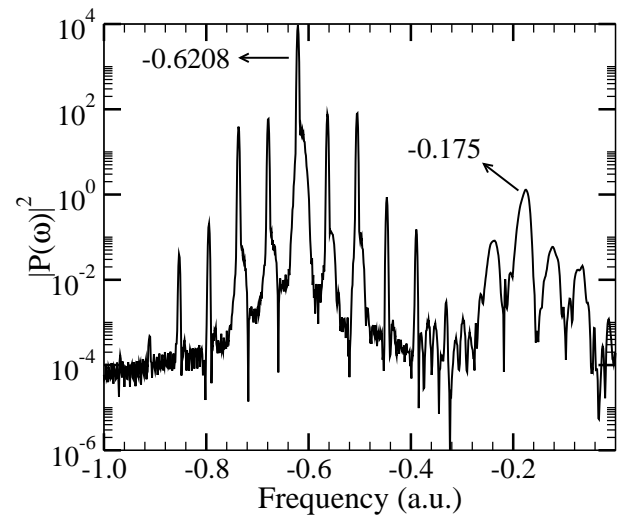


FIG. 5: The quasienergies of H_2^+ in the presence of an intense laser field. The power-spectral density of the autocorrelation function is shown for a range of angular frequencies. In this case $\lambda = 800$ nm, $I = 5 \times 10^{14} \text{ W cm}^{-2}$ and $R = 2$ a.u. .

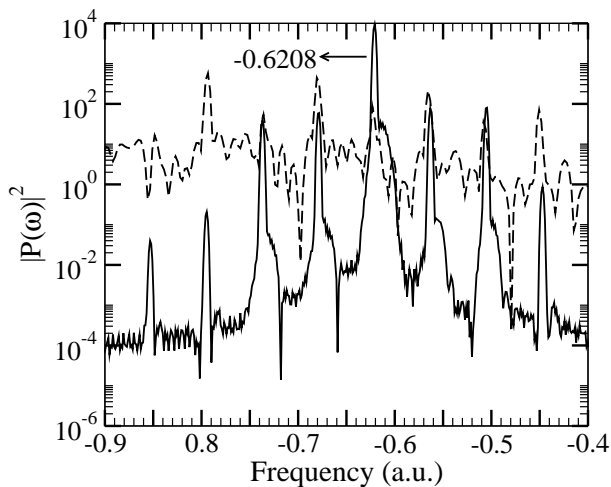


FIG. 6: Spectral density of the correlation function showing the quasienergy spectrum. Comparison of the quasienergies of H_2^+ in the presence of intense laser field using different gauges. Here, $\lambda = 800$ nm, $I = 5 \times 10^{14}$ W cm^{-2} and $R = 2$ a.u.. —, length gauge; - - -, velocity gauge.

results obtained using the velocity-gauge are also shown in figure 6. Both spectra have the same spectral line structure over the domain shown in the figure. The method is quite useful for calculation of isolated resonance shifts. However when overlapping resonances are present, for example at larger values of R the resultant spectrum is very unclear and the method breaks down.

C. Ionization of positronium

The code can be easily adapted to the ionization of positronium in an intense laser field. An investigation of this kind has been made by Madsen *et al* [19] using a time-dependent basis-set expansion. The scaling factor h_ρ is adjusted to be 0.52085 for Ps with $\Delta z = 0.1$ a.u. and $N_\rho = 30$ to optimize the ground state energy to -0.250000001 a.u.. For the sake of comparison [19], the velocity gauge is used and the pulse is taken as

$$A(t) = A_0 \sin^2\left(\frac{\pi t}{T_p}\right) \sin(\omega_L t), \quad (43)$$

where $A_0 = F_0/\omega_L$ with F_0 the peak electric field strength. We take a pulse duration $T_p = 50$ fs and a wavelength $\lambda = 780$ nm. The ionization probability versus laser intensity is shown in figure 7. Our results are in very good agreement with those of Madsen *et al* [19] over a wide range and especially for the intermediate intensities.

D. Ionization rates for H_2^+ by intense infrared light

At very high intensities the bound states will ionize extremely quickly with a non-exponential decay. While the ionization rate or width Γ is mathematically well-defined, one

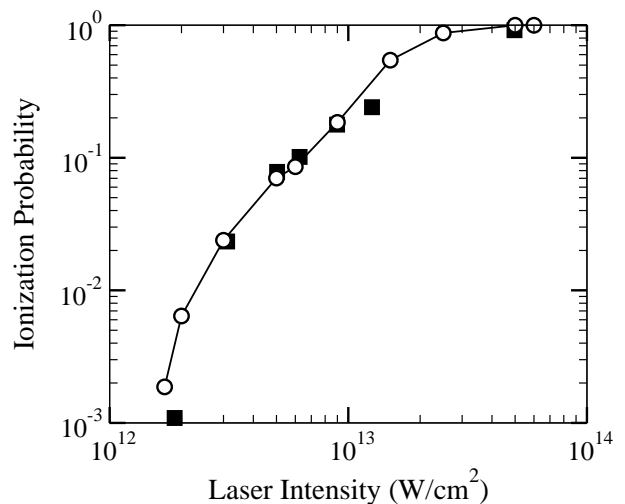


FIG. 7: Ionization probability of Positronium at different laser intensities for wavelength $\lambda = 780$ nm and pulse duration $T_p = 50$ fs. \circ Present Calculations; \blacksquare Results of Madsen *et al.* [19].

cannot calculate the rate so easily from observation of population decay. In physical terms, in an experiment this corresponds to saturation, that is the molecules fully ionize before the pulse has finished. In this case it is difficult for experiments to analyse the response of the system. This requires extremely short pulses, with associated rapidly-varying pulse envelope and broad bandwidth. Under such circumstance a time-dependent treatment is indispensable. The fragmentation of H_2^+ by an intense infrared laser ($\lambda = 790$ nm) is a problem of current interest. For an intensity $I = 3 \times 10^{15}$ W cm^{-2} , and $R = 5$ a.u. the ionization rate is roughly 5.5fs^{-1} . Thus the molecule will be fully ionized within a fraction of an optical cycle. Mathematically, the ionization rates in this regime can be calculated by scaling as shown by Madsen *et al.* [19]. Using the arbitrary dimensionless parameters α and β we can change the scale of length and time according to

$$\tilde{r} = \alpha\beta r, \quad \tilde{t} = \alpha\beta^2 t, \quad (44)$$

so that

$$\tilde{\omega} = \alpha^{-1}\beta^{-2}\omega_L. \quad (45)$$

The corresponding TDSE becomes

$$i\frac{\partial}{\partial \tilde{t}}\psi(\tilde{\rho}, \tilde{z}, \tilde{t}) = \left[-\frac{\alpha}{2\mu} \left(\frac{\partial^2}{\partial \tilde{z}^2} + \frac{\partial^2}{\partial \tilde{\rho}^2} + \frac{1}{\tilde{\rho}} \frac{\partial}{\partial \tilde{\rho}} \right) + \tilde{V}_e(\tilde{R}, \tilde{\rho}, \tilde{z}) + \tilde{V}_{l-m}(\tilde{z}, \tilde{t}) \right] \psi(\tilde{\rho}, \tilde{z}, \tilde{t}), \quad (46)$$

TABLE IV: Test of the scaling procedure. Ground-state energies and the corresponding ionization rates are calculated using scaled ($\alpha = 1.43$, $\beta = 1.43$) and unscaled Hamiltonians. The laser parameters are $\lambda=800$ nm and $I=3.2 \times 10^{14}$ W cm $^{-2}$ and a range of bond lengths R are considered. Energy is in atomic units, ionization rate in fs $^{-1}$ and R in atomic units.

R	Scaled model		Unscaled model	
	Energy	Rate	Energy	Rate
4.0	-0.54600	0.128	-0.54608	0.138
5.0	-0.52442	0.168	-0.52442	0.165
6.0	-0.51185	0.341	-0.51199	0.351
7.0	-0.50532	0.299	-0.50559	0.294
8.0	-0.50232	0.289	-0.50257	0.264
9.0	-0.50112	0.211	-0.50119	0.196

with

$$\begin{aligned} \tilde{V}_e(\tilde{R}, \tilde{\rho}, \tilde{z}) = & -\frac{Z_1}{\beta\sqrt{\tilde{\rho}^2 + (\tilde{z} - \tilde{R}/2)^2}} \\ & -\frac{Z_2}{\beta\sqrt{\tilde{\rho}^2 + (\tilde{z} + \tilde{R}/2)^2}} \\ & + \frac{\alpha\Lambda^2}{2\tilde{\rho}^2} + \frac{Z_1 Z_2}{\beta\tilde{R}}, \end{aligned} \quad (47)$$

and

$$\tilde{V}_{l-m}(\tilde{z}, \tilde{t}) = \alpha^2 \beta^3 \tilde{z} E(\tilde{\omega}, \tilde{t}). \quad (48)$$

The laser intensity and the ionization rate scale as

$$\tilde{I} = \alpha^{-4} \beta^{-6} I, \quad (49)$$

and

$$\tilde{\Gamma} = \alpha^{-1} \beta^{-2} \Gamma, \quad (50)$$

accordingly.

The numerical stability scaling can be tested at intensities below saturation. In table IV, we compare the scaled ground-state energies and ionization rates obtained with those from a direct calculation for $\lambda = 800$ nm and $I = 3.2 \times 10^{14}$ W cm $^{-2}$ at various internuclear distances. The agreement is reasonable with relative errors in ionization rates below 9%. The values of the scaling parameters in this case are $\alpha = 1.43$ and $\beta = 1.43$. The interest in obtaining rates at high intensity follows experimental work that estimated the bond length dependence of ionization rate from the ion energy spectrum [20, 21]. Our results are compared with experimental spectra in figures 8 and 9 taking $\alpha = 1.43$ and $\beta = 1.43$. The experimental measurements collect ions over a large part of the focal volume, and hence we adjust the normalization of the data to the theoretical results. It is surprising and remarkable to note that both spectra, experimental and theoretical, are dominated by a single large peak and that its location is reproduced accurately by the theory. For $R < 7$ the shape of the ionization rate is quite well reproduced. This is surprising in

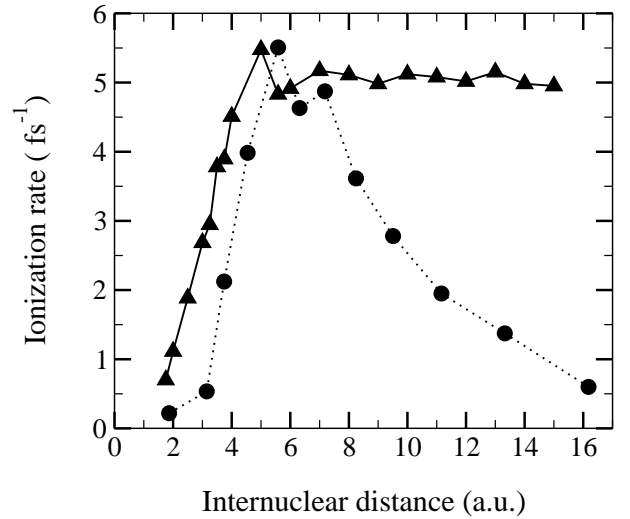


FIG. 8: Ionization rates as a function of internuclear distance (R) with $\lambda = 790$ nm and $I = 3 \times 10^{15}$ W cm $^{-2}$. \blacktriangle , theoretical calculations using Hamiltonian rescaling procedure; \bullet , experimental measurements [21]. The experimental data are normalized to the theoretical result at $R = 5$ a.u..

view of the fact that the theoretical model is greatly simplified and does not include nuclear vibrations nor the averaging over molecular orientation and focal volume as would be required for a true comparison. One conclusion might be that the extremely good agreement indicates that the ionization rate is a strongly-peaked function of bond length, molecular orientation and laser intensity so that the averaging process does not broaden these features. For internuclear distance greater

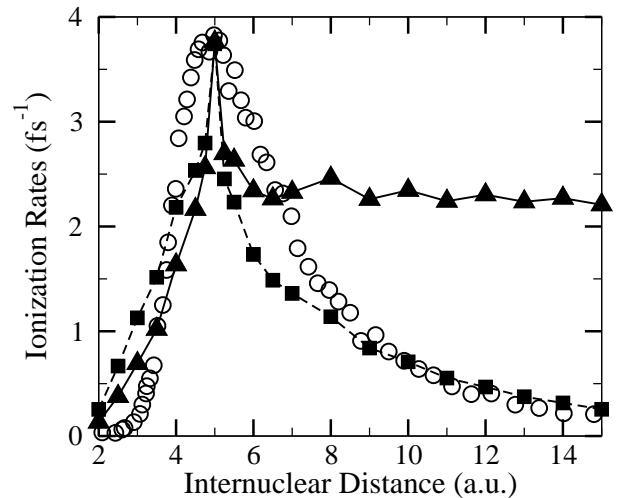


FIG. 9: Ionization rates as a function of internuclear distance (R) with $\lambda = 800$ nm and $I = 1.4 \times 10^{15}$ W cm $^{-2}$. \blacktriangle , theoretical calculations using Hamiltonian rescaling procedure; \blacksquare , theoretical modelling with population depletion based on Coulomb explosion included, $dP/dR \approx -C(\Gamma/v)P$, where we take the constant $C = 0.2$; \circ , experimental measurements [20]. The experimental data are normalized to the theoretical result at $R = 5$ a.u..

than 7 a.u., there is no dependence on bond length, indicating the loss of molecular effects. An essential assumption in the theoretical model is that the molecules are equally populated at all R corresponding to the ionization process occurring as the molecule dissociates at steady speed. An explanation of the experimental shortfall in ions from large R is that if the molecule ionizes fully at smaller R it cannot survive to yield ions at large bond lengths and the ion yield rapidly drops. The other point in figure 8 deserving note is the overall leftward displacement of our theoretical curve compared with the experimental one. There is the possibility that the experimental calibration of the laser intensity underestimates the actual intensity experienced by the molecules. A very rough simulation of the molecule depletion is shown in figure 9 in which the theoretical ion yield is exponentially attenuated. The curve shown is $P(R) = \Gamma(R) \exp(-C \int_{R_0}^R \Gamma(R)/v(R) dR)$ where $v(R)$ is the relative velocity of the ions taken to be the classical value for Coulomb repulsion $m_p v^2/4 + 1/R_0 = 1/R$. The factor C is an empirical constant taken to fit to the experimental curve in figure 9. We find $C \sim 0.2$ gives the best shape for the distribution. Taking $C = 1$ leads to a severe loss of ions at large R , almost no ions survive beyond $R = 7$ in this approximation. Of course one might expect that the low intensity focal averaging process might raise the yield of ions from large R and give a more realistic picture of the process. This would require inclusion of the attenuation corrections discussed above. Nonetheless, it is fair to compare this theory and experiment for small R values, and in this respect the agreement is remarkably good.

V. CONCLUSIONS

We have made a detailed investigation of a method which is designed to solve the reduced-dimensionality time-dependent Schrödinger equation for metastable systems in intense fields. We have checked the reliability of the present code by examining the convergence and the gauge dependence. Applications to several problems have been carried out and yield good agreement with other available theoretical results. However, by direct solution of the TDSE, our method can be applied to both short and long pulses and to a large variety of wavelengths. The provision of parallel computer architecture offers the opportunity to study such systems from first principles and in full dimensionality.

Acknowledgements

LYP acknowledges the award of a PhD research studentship from the International Research Centre for Experimental Physics (IRCEP) at Queen's University Belfast. DD acknowledges the award of an EPSRC Postdoctoral Fellowship in Theoretical Physics. This work has also been supported by a grant of computer resources at the Computer Services for Academic Research, University of Manchester and at HPCx, Daresbury Laboratory provided by EPSRC to the UK Multiphoton, Electron Collisions and BEC HPC Consortium.

-
- [1] K. Codling and L. J. Frasinski, *J. Phys. B: At. Mol. Opt. Phys.*, **26**, 783 (1993).
 - [2] A. Giusti-Suzor, F. H. Mies, L. F. DiMauro, E. Charron and B. Yang, *J. Phys. B: At. Mol. Opt. Phys.*, **28**, 309 (1995).
 - [3] J. H. Posthumus, *Molecules and Clusters in Intense Laser Fields* (Cambridge: Cambridge University Press, 2001), ch2.
 - [4] V. P. Krainov and M. B. Smirnov, *Phys. Rep.*, **370**, 237 (2002).
 - [5] G. G. Paulus, F. Grasbon, H. Walther, P. Villorresi, M. Nisoli, S. Stagira, E. Priori and S. De Silvestri, *Nature*, **414**, 182 (2001).
 - [6] S. Chelkowski and A. D. Bandrauk, *J. Phys. B: At. Mol. Opt. Phys.*, **28**, L723 (1995).
 - [7] E. S. Smyth, J. S. Parker and K. T. Taylor, *Comput. Phys. Commun.*, **114**, 1 (1998).
 - [8] D. Dundas, *Phys. Rev. A*, **65**, 023408 (2002).
 - [9] G. L. Ver Steeg, K. Bartschat and I. Bray, *J. Phys. B: At. Mol. Opt. Phys.* **36**, 3325 (2003).
 - [10] D. Dundas, K. J. Meharg, J. F. McCann and K. T. Taylor, *Eur. Phys. J.: D*, **26**, 51 (2003).
 - [11] L.-Y. Peng, D. Dundas, J. F. McCann, K. T. Taylor and I. D. Williams, *J. Phys. B: At. Mol. Opt. Phys.*, **36**, L295 (2003).
 - [12] D. Baye and P.-H. Heenen, *J. Phys. A: Math. Gen.*, **19**, 2041 (1986).
 - [13] D. Dundas, J. F. McCann J F, J. S. Parker and K. T. Taylor, *J. Phys. B: At. Mol. Opt. Phys.*, **33**, 3261 (2000).
 - [14] W. E. Arnoldi, *Quart. Appl. Math.*, **9**, 17 (1951).
 - [15] T. E. Sharp, *Atomic Data*, **2**, 150 (1971).
 - [16] M., Plummer and J. F. McCann, *J. Phys. B: At. Mol. Opt. Phys.*, **29**, 4625 (1996).
 - [17] M., Plummer and J. F. McCann, *J. Phys. B: At. Mol. Opt. Phys.*, **30**, L401 (1997).
 - [18] A. Maquet, Shih-I Chu and W. P. Reinhardt, *Phys. Rev. A*, **27**, 2946 (1983).
 - [19] L. B. Madsen, L. A. A. Nikolopoulos and P. Lambropoulos, *Eur. Phys. J.: D*, **210**, 67 (2000).
 - [20] G. N. Gibson, M. Li, C. Guo and J. Neira, *Phys. Rev. Lett.*, **79**, 2022 (1997).
 - [21] I. D. Williams, P. McKenna, B. Srigengan, I. M. Johnston, W. A. Bryant, J. H. Sanderson, A. El-Zein, T. R. J. Goodworth, W. R. Newell, P. F. Taday and A. J. Langley, *J. Phys. B: At. Mol. Opt. Phys.*, **33**, 2743 (2000).